Volume 1 | Number 1 | Jan 2013 | Pages 1–100

Food & Function

Linking the chemistry and pyhsics of food with health and nutrition
www.rsc.org/foodfunction

ROYAL SOCIETY OF CHEMISTRY

ROYAL SOCIETY OF CHEMISTRY

www.rsc.org/foodfunction

1

1 **Modelling of nutrient bioaccessibility in almond seeds based on**

2 **the fracture properties of their cell walls**

3

4 Terri Grassby,[†a] David R. Picout,[†a] Giuseppina Mandalari,[b,c] Richard M.

5 Faulks,[b] Cyril W.C. Kendall,[d,e] Gillian T. Rich,[b] Martin S.J. Wickham,[f] Karen

6 Lapsley,[g] and Peter R. Ellis[*a]

7 *[a]King's College London, Diabetes and Nutritional Sciences Division, Biopolymers Group,*

8 *Franklin-Wilkins Building, 150 Stamford Street, London SE1 9NH, United Kingdom*

9 *[b]Model Gut Platform, Institute of Food Research, Norwich NR4 7UA, United Kingdom*

10 *[c]Department of Drug Science and Products for Health, University of Messina, Viale.*

11 *Annunziata, 98168 Messina, Italy*

12 *[d]Nutritional Sciences and [e]Medicine, Faculty of Medicine, University of Toronto, Toronto,*

13 *Ontario M55 3E2, Canada*

14 *[f]Nutrition Research, Leatherhead Food Research, Randalls Road, Leatherhead, Surrey KT22*

15 *7RY, UK*

16 *[g]Almond Board of California, 1150 9th Street, Suite 1500, Modesto, CA 95354, USA*

17

18 <u>Running Title:</u>   Theoretical model predicts lipid bioaccessibility from almonds

19

20 [*]Corresponding author. Tel.: +44 (0) 207 848 4238; fax: +44 (0) 207 848 4171. *E-mail*

21 *address*: peter.r.ellis@kcl.ac.uk (P.R. Ellis). *Postal address*: Biopolymers Group, Diabetes

22 and Nutritional Sciences Division, King's College London, Franklin-Wilkins Building

23 (Room 4.102), 150 Stamford Street, London, SE1 9NH, UK.

24 [†]Co-first authors.

25 **Abstract**

26 The cell walls (dietary fibre) of edible plants, which consist of mainly non-starch

27 polysaccharides, play an important role in regulating nutrient bioaccessibility (release) during

28 digestion in the upper gastrointestinal tract. Recent studies have shown that structurally-

29 intact cell walls hinder lipid release from the parenchyma cells of almond seeds. A

30 theoretical model was developed to predict the bioaccessibility of lipid using simple

31 geometry and data on cell dimensions and particle size for calculating the number of ruptured

32 cells in cut almond cubes. Cubes (2 mm) and finely-ground flour of low and high lipid

33 bioaccessibility, respectively, were prepared from almond cotyledon. The model predictions

34 were compared with data from *in vitro* gastric and duodenal digestion of almond cubes and

35 flour. The model showed that lipid bioaccessibility is highly dependent on particle size and

36 cell diameter. Only a modified version of the model (the Extended Theoretical Model,

37 ETM), in which the cells at the edges and corners were counted once only, was acceptable for

38 the full range of particle sizes. Lipid release values predicted from the ETM were 5.7% for

39 almond cubes and 42% for almond flour. *In vitro* digestion of cubes and flour showed that

40 lipid released from ruptured cells was available for hydrolysis and resulted in lipid losses of

41 9.9 and 39.3%, respectively. The ETM shows considerable potential for predicting lipid

42 release in the upper gastrointestinal tract. Further work is warranted to evaluate the efficacy

43 of this model to accurately predict nutrient bioaccessibility in a broad range of edible plants.

44

45 *Keywords:* Plant cell walls; Non-starch polysaccharides; Almond; Nutrient bioaccessibility;

46 Microstructural analysis; Mathematical modelling.

47

48

1. Introduction

There is considerable interest in investigating the structure and properties of plant cell walls and their constituent polysaccharides in the biological and biomedical fields. This includes examining the role of cell walls and their components in human nutrition,[1-3] animal feed science[4] and, more recently, in palaeoethnobotany, in relation to the evolution of the human diet, digestion and metabolism.[5-7] Also, cell walls are of industrial and economic importance in the production of bioethanol and other renewable biofuels.[8,9]

Plant cell walls are supramolecular assemblies of cellulose, hemicelluloses, pectic substances, non-carbohydrate components and water.[3] The amounts and relative proportions of non-starch polysaccharides (NSP) and other components in cell walls vary depending on botanical source and factors such as the type, function and maturity of plant tissue. The heterogeneity in composition and structure of individual NSP, as well as the covalent and non-covalent linkages between polysaccharide chains in the cell wall matrices, explain the wide variation in cell wall properties, e.g. fracture mechanics, disassembly during ripening and dissolution of individual polymers.[10-14] The non-carbohydrate components (e.g. protein, polyphenolics, cutin) are present as minor components in cell walls, but some form covalent cross links with the cell wall polysaccharides and significantly modify their properties and biological activity.[15]

It is well established that the cell walls of plant foods, more commonly referred to as dietary fibre, have potential beneficial effects on health and disease prevention, such as reduced risk factors associated with type 2 diabetes,[2] coronary heart disease (CHD)[16] and cancer.[17] These beneficial effects are strongly linked to the properties of cell walls and individual cell wall polysaccharides in the gastrointestinal (GI) tract, which impact on gut functions such as gastric emptying, digestion kinetics and microbial fermentation.[1-3,11]

73   One major challenge is to understand the mechanisms by which intact cell walls regulate

74   the bioaccessibility of nutrients from plant foods during digestion.[11,18] Bioaccessibility is

75   defined here as the proportion of a nutrient or phytochemical "released" from a complex food

76   matrix and, therefore potentially available for digestion and/or absorption in the GI tract. In

77   edible plant tissues, the cell walls are resistant to degradation by endogenous gut enzymes

78   (e.g. α-amylase) and can therefore play an important role in regulating bioaccessibility.[2,3,19]

79   However, the mechanisms by which cell wall structure and properties influence nutrient

80   release are not well understood.[11,20,21] Previous studies have highlighted the importance of

81   the structural integrity of cell walls, but have not addressed the crucial issue of quantifying

82   bioaccessibility.[20,22-24]

83   The way plant tissues break down during physical disruption (e.g. milling, mastication) is

84   dependent on a number of factors, notably cell wall strength and inter-cell adhesion, which in

85   turn is dependent on the composition and structure of cell walls. For example, crisp/crunchy

86   fruits and vegetables exhibit cell wall rupture when triturated, whereas, following

87   hydrothermal processing, most edible plants will soften because of cell separation, due to the

88   weakening of the cell-cell adhesion associated with the pectic polysaccharides.[3] The

89   proportion of cells ruptured in plant tissue is dependent on the area of fractured surfaces

90   created by mechanical processing and/or mastication.[20] After ingestion, the released nutrients

91   are exposed to the enzyme-rich environment of the gut lumen and are therefore potentially

92   available for digestion and absorption.[21] For intact cells, intra-cellular nutrients are

93   encapsulated and so the permeability of cell walls is likely to be a more important property

94   involved in modifying nutrient release.

95   In earlier studies we showed that during digestion any intact almond cell walls inhibit the

96   release of intra-cellular lipid and other nutrients.[20,21] The mastication of almond tissue

97   produced fractured surfaces of ruptured parenchyma cells with intra-cellular nutrients

98   exposed to the digestive fluids and therefore more available for digestion. However, the

99   lipid-rich parenchyma cells beneath the fractured cell layer were found to be largely intact

100   after grinding, cutting and mastication,[20] so that cell walls seem to act as a physical barrier to

101   nutrient release and digestion.[21]

102   In this study we have investigated the release of lipid from almond seeds by developing a

103   predictive model of lipid bioaccessibility. Our motivation for selecting almonds as a *'model*

104   *food'* is that presently there is intense interest in the effect of this tree nut on lipid and energy

105   metabolism and its possible long term health benefits. Previous human studies have shown

106   that almonds decrease fasting plasma concentrations of LDL- and oxidised-LDL cholesterol,

107   postprandial glycaemia and insulinaemia, and oxidative damage.[25-27] A more recent study of

108   almonds has now provided compelling evidence for the importance of cell wall integrity in

109   attenuating postprandial lipaemia,[16] which itself is associated with a reduced risk of CHD.[28]

110   Paradoxically, despite the high lipid (energy) concentration of almonds, it has been reported

111   that adding almonds to a habitual diet does not necessarily result in weight gain and may even

112   facilitate weight loss.[29-31] Explanations for these observations are likely to include impaired

113   bioaccessibility and digestion of almond lipid, leading to increased excretion of faecal fat and

114   perhaps also the satiating effect of firstly cell walls[20,29,32] and secondly, activation of the ileal

115   brake by undigested nutrients reaching the terminal ileum (see review by Maljaars et al).[33]

116   Previous modelling studies of lipid-bearing seeds have focused only on the efficiency of

117   oil extraction using solvents such as supercritical carbon dioxide[34,35] and are therefore of

118   limited use in predicting lipid bioaccessibility. In the present study, we have constructed two

119   variants of a theoretical model for predicting lipid release from ruptured cells. The model

120   variants are based on geometric principles, almond microstructure and the application of a

121   stereological method to almond cell dimensions. Bioaccessibility values predicted from the

122   model variants were compared with data obtained from an *in vitro* digestion assay,[21] and also

123   an *in vivo* mastication study.[36] The potential use of theoretical predictions for estimating

124   lipid bioaccessibility *in vivo* and its applicability to other foods was also evaluated.

2. Materials and Methods

2.1. Development of a theoretical model

127   Two variants of a theoretical model were constructed to predict the bioaccessibility of lipid

128   from ruptured parenchyma cells of almond cotyledons. The development of the model was

129   originally based on geometry and cell packing theory in combination with measurements of

130   cell dimensions and intra-cellular lipid content. Thus, using methods described below, the

131   following information was obtained for initial model construction: (a) the dimensions of

132   lipid-containing parenchyma cells; (b) the packing arrangement of cells in the cotyledon; (c)

133   the amount of lipid within the cells; (d) the number of cells ruptured by cutting the almond

134   tissue into a defined geometry (i.e. cubes); and (e) the size of the cubes.

135   Previous work on masticated, digested and mechanically processed almonds indicated

136   that only cells that are ruptured have the capacity to immediately release lipid, with little

137   evidence of release from intact cells, in which lipid bodies remained encapsulated by cell

138   walls.[20,21,36] Therefore, to construct the predictive model it was assumed that ruptured cells

139   on fractured surfaces are the only cells that contribute to lipid release, at least post-

140   mastication[20,36] and in the early stages of digestion.[21] In other words, early lipid release is

141   directly proportional to the number of broken cells created during cutting or mastication.

142   To estimate the proportion of ruptured cells, relative to those that are intact, it was

143   essential to define a simple geometry of almond cotyledon for model development. Thus,

144   cotyledon cubes of defined size were selected for the initial construction of the model. The

145   number of intact and fractured cells in these '*theoretical*' cubes was estimated using

146   information on shape, size and packing arrangement of the parenchyma cells. There were

147   also practical advantages to using real cubes in digestibility experiments *in vitro* and *in vivo*,

148   as described in our previous paper.[21] A schematic illustration of an almond seed (Fig. 1)

149   shows how the cubes were derived from the cotyledon tissue (i.e. without the brown-

150   pigmented seed coat or skin) and highlights the characteristics of the fractured surfaces. The

151   cube surfaces, which are presented as scanning electron microscopy (SEM) images (for

152   method see Section 2.3 and Ellis et al.[20]) superimposed on the cartoon, show ruptured

153   parenchyma cells, some of which are hidden by larger lipid droplets formed from the

154   coalescence of intra-cellular lipid bodies (i.e. oleosomes).

155   **2.2. Source and chemical composition of almonds and preparation of almond cubes**

156   Natural (raw) almond seeds (*Amygdalus communis* L; variety, Nonpareil) and almond flour,

157   prepared from the same batch of almond seeds, were produced by Steward & Jasper Orchards

158   (Newman, CA, USA) and kindly provided by the Almond Board of California (ABC;

159   Modesto, CA, USA) and stored at 3-5˚C. Almond seeds are referred to as kernels by almond

160   growers and processors. Details of methods for chemical analysis, including cell wall

161   polysaccharides of almonds, are described in previous papers.[20,21] The nutrient content of the

162   almond seeds was as follows: moisture, 5.5%; protein (Kjeldahl, N x 5.71), 21.2%; lipid

163   (Soxhlet; *n*-hexane), 55.2%; available carbohydrate (mainly sugars), 5.5%; and ash (total

164   minerals), 3.1%. Cell wall analysis showed that the main sugars (expressed as mol %) were

165   arabinose (39.9%), glucose (16.7%), galacturonic acid (21.2%) and xylose (12.0%),

166   indicating that the main polysaccharides present were cellulose, pectic material (arabinan and

167   galacturonan) and xyloglucan, as previously suggested.[20,21]

168   The natural almond cube samples, used for the *in vitro* digestion study, were prepared by

169   carefully cutting the almond cotyledon into cubes of 2 mm dimension. Each seed was

170 separated to yield two cotyledons, each cotyledon having one flat and one curved surface.

171 The sides were planed off with a microtome blade and then the remaining cotyledon was cut

172 into 2 mm square lengths and subsequently 2 mm cubes using a razor-blade guillotine.

173 Almond flour was prepared by fine grinding of the same variety and batch of almonds, in

174 which the seed coat (testa) or "skin" had been removed. The particle size distribution of the

175 flour was determined by mechanical sieving; the mean particle size value for the flour was

176 200 μm (data provided by ABC) and 250 μm as measured in our laboratory.[13]

177 2.3. Physical characterisation of almond parenchyma tissue and cells

178 Microstructural analysis of almond cotyledon tissue was performed using light microscopy

179 (LM), SEM and transmission electron microscopy (TEM), as detailed previously.[20] Almond

180 cotyledon tissue was rapidly fixed in 1% (w/v) osmium tetroxide and then added to 2.5%

181 (v/v) glutaraldehyde in 0.1 M sodium cacodylate buffer (pH 7.2) and left overnight. The

182 samples were subsequently washed twice in 0.1 M sodium cacodylate buffer and post-fixed

183 in 1% (w/v) osmium tetroxide for 2 h. The almond samples were dehydrated in ethanol serial

184 dilutions: 50%, 70% and 90% (v/v) ethanol in distilled water for 30 min for each solution and

185 finally in 100% (v/v) ethanol for 30 min (3 times). For LM and TEM, the samples were

186 infiltrated with Spurr resin and embedded in moulds and polymerised at 60˚C. Sections of 1

187 μm for LM were cut on a Reichert Ultracut ultramicrotome (Leica Microsystem Ltd, UK) and

188 then mounted on glass slides and stained in 1% (w/v) toluidine blue. Ultra-thin sections of

189 ~70 nm were cut for TEM and images were viewed on a JEOL 100CX Mk. II transmission

190 electron microscope (JEOL Ltd, UK). Samples examined by SEM were critical point dried in

191 a Polaron E3000 CP Drier (Quorum Technologies, UK), mounted on stubs and sputter coated

192 with gold in a Polaran E5100 sputter coating unit and viewed on a JOEL 25SM and a Philips

193 501 scanning electron microscope (FEI Company, UK).

194   The dimensions of individual lipid-bearing parenchyma cells (n = 320) were determined

195   by examining with LM and TEM. Image analysis (SIS software) of micrographs produced

196   from transverse and longitudinal sections of the seeds was used to determine the surface area

197   of parenchyma cell profiles and also to quantify the lipid content of the cells (see Section

198   2.5). The 'profile' cell diameters were calculated from the 'profile' surface area data using

199   simple geometry (i.e. area of a circle). The mass, volume and density of almond cotyledon

200   were determined, with volume being estimated by geometric theory and a water displacement

201   method.

202   The mean profile diameter of spherical cells, sectioned by a random plane, rarely

203   corresponds to the real diameter of the parenchyma cell. Therefore, a stereological method,[37]

204   which allows a 3-D interpretation of 2-D planar sections of the parenchyma tissue, was used

205   to estimate the real cell diameter from the profile diameter determined by microscopy.

206   Previous observations of the almond parenchyma cells by microscopy indicated that they are

207   largely spherical in shape, albeit slightly distorted.[20] In spheres of equal size the profile

208   diameter cut by a random plane varies and depends on where the sphere is intersected.[37]

209   Thus, the profile diameter is largest around the equator and becomes smaller as the sectioned

210   plane moves towards the poles. Fig. 2 illustrates this effect schematically using spheres to

211   represent almond parenchyma cells. Weibel described a linear relationship between sphere

212   size and mean profile size, which was used to calculate sphere diameter from a measurement

213   of profile diameters, as expressed in the following equation:[37]

214
$$d = \frac{4}{\pi} d'$$
(1)

215   where d represents the real diameter of the sphere (e.g. parenchyma cell) and d' the

216   measured mean profile diameter (as estimated from microscopy analysis).

217 **2.4. Number and packing density of parenchyma cells in almond tissue of defined**

218 **geometry**

219 The total number of parenchyma cells contained in cubes of almond cotyledon was estimated

220 using information on the shape, size and packing density of the cells. On the assumption that

221 parenchyma cells approximate to spheres, sphere packing theory can be used to estimate the

222 packing density of the cells.[38-40]

223 **2.5. Content and distribution of lipid in almond parenchyma cells**

224 For individual parenchyma cells of almond cotyledon, image analysis of micrographs,

225 obtained from TEM of ultra-thin sections of cotyledon tissue, was performed to estimate

226 intra-cellular lipid. Parenchyma cells were randomly selected from all areas of the sections

227 and the total surface area of each cell profile and its intra-cellular contents was determined.

228 The lipid value was calculated as the difference between the total surface area of the cell

229 profile and the surface area of non-lipid components (e.g. protein), and expressed as a

230 percentage of the total cell profile surface area. The lipid content of cells was then calculated

231 as a percentage volume. To estimate mass from volume, a density value for almond oil

232 (0.91 g/cm^3) was used.[41] Total lipid analysis of whole almond seeds was carried out as

233 described above (Section 2.2).

234 **2.6. In vitro lipid digestion experiment**

235 The *in vitro* digestion assays of lipid in 2 mm cubes and finely-ground flour of raw almond

236 seeds were performed as described in detail by Mandalari et al.[21] This experiment was

237 designed to study mass loss of lipid from almonds during *in vitro* digestion under both gastric

238 and duodenal conditions (a total of 3 h digestion). Carefully cut cubes (2 mm) of almond

239 cotyledon and finely-ground almond flour (1.5 g amounts) were prepared (see Section 2.2)

240 and used for the *in vitro* digestion assay. These samples represent almond particles that

241 contain nutrients of low and high bioaccessibility (i.e. cubes and flour, respectively),

242 reflecting large differences in the proportion of ruptured cells relative to intact cells. The idea

243 of using other cube sizes (<2 mm) for the *in vitro* digestion assay was rejected for a number

244 of reasons, notably the practical limitations in producing homogeneous batches of cubes over

245 a broad size range, especially at sizes <1 mm. Assuming that acceptable 1 mm cubes could

246 be produced, the predicted bioaccessibility value of these would only be ~11%.

247   Each digestion assay was performed four times and after each experiment solid digested

248 almond material was recovered for lipid analysis. Total lipid loss, as a percentage of original

249 lipid content of the almond seeds, was then determined for the digested almond samples and

250 compared with predictions of the theoretical model for lipid bioaccessibility of the same

251 samples.

252 3. Results

253 3.1. Size, shape and packing density of almond seed parenchyma cells

254 Microstructural examination of almond sections showed that each cotyledon consisted

255 primarily of thin-walled (1–3 µm, thickness) parenchyma cells (Fig. 3a), each of which

256 contained numerous intra-cellular lipid bodies (~1-3 μm, diameter), as observed

257 previously.[20,42,43] Most of the parenchyma cells were of similar size and shape (i.e. relatively

258 monodisperse). The parenchyma cells examined in this study were characterised as being

259 slightly deformed spheres (Fig. 3a), i.e. pseudo-spherical, which is consistent with earlier

260 micro-structural observations.[20,42,43] Therefore, to simplify the calculations for constructing

261 the model, the parenchyma cells were deemed to be 'spherical'. Surface area data, obtained

262 from image analysis of individual parenchyma cell profiles, was used to calculate profile

263 diameters (d') by simple 2-D geometry, producing a mean profile diameter ($\pm$SD) of 28$\pm$ 6

264 µm (n=320; range 15-40 µm). The real diameter (d) of the parenchyma cells, calculated from

265 the profile diameters using eqn (1), was estimated to have a mean value of 36 µm (range

266 19.1-50.9 μm).

267 **3.2. Content and distribution of lipid in almond parenchyma cells**

268 The mean percentage ($\pm$ SD) of lipid in a cell, determined by image analysis of TEM

269 micrographs (Fig. 3b), was found to be 66.4 $\pm$ 5.6% (n=35). The percentage lipid values,

270 calculated as the difference between the total cell surface area and surface area of the non-

271 lipid components, were reasonably consistent in all the TEM images (both longitudinal and

272 transverse sections), indicating that the distribution of cell contents was relatively

273 homogeneous. It was reasonable to assume therefore that the percentage lipid values are

274 representative of lipid volume, and therefore mass. The mean value for lipid mass in the

275 parenchyma cells of almond cotyledon was estimated to be ~60.4%. After allowing for the

276 contribution from the almond seed coat (~3-4%, w/w), the mean value for lipid in the whole

277 almond seed was estimated to be 55%. This value is reassuringly close to the total lipid

278 content of almonds obtained by standard solvent-extraction methods seen in the present paper

279 (section 2.2) and also reported previously.[20,21]

280 **3.3. Construction of model variants for predictions of bioaccessibility**

281 The construction of the two variants of the model was based on the same underlying concept,

282 namely that the proportion of ruptured cells in any given particle could be used as a way of

283 estimating lipid release, as per eqn (2). This is the basis for the Simplified Theoretical Model

284 (STM). The Extended Theoretical Model (ETM) includes two additional terms, which

285 account for cells at the edges and corners being part of more than one cut face.

286 *Lipid release (%) = (mass of lipid released / mass of lipid in sample) × 100* (2)

287   For both variants of the model, it was assumed that the cells were spherical and

288   monodisperse, that the particles were cubes and that lipid is evenly distributed throughout the

289   almond. The following equations were considered during initial model construction:

290 $$Mass\ of\ lipid\ in\ almond\ sample = m \times L_w \tag{3}$$

291 $$Number\ of\ cubes\ in\ almond\ sample = \frac{m}{p^3 \times \rho} \tag{4}$$

292 $$Mass\ of\ lipid\ in\ cube = L_w \times p^3 \times \rho \tag{5}$$

293 $$Average\ number\ of\ cells\ in\ a\ cube, \langle N_c \rangle = \frac{p^3}{\frac{4}{3}\pi\left(\frac{d}{2}\right)^3} \times P \tag{6}$$

294   where m = mass of almond sample (mg), P = packing density of parenchyma cells in a

295   cube, d = the mean real diameter of a parenchyma cell (μm), p = the size of the almond

296   cubes (μm), ρ = the density of almond cotyledon (g/cm^3) and L_w = the percentage of lipid

297   by weight in almond cotyledon. The real cell diameter (d) of a cell was estimated from the

298   profile diameter (d') using eqn (1).

299   As seen in eqn (6), the average number of cells in a cube, $\langle N_c \rangle$, was estimated by dividing the

300   volume of a cube by the volume of a cell, taking into account the packing density of the cells.

301   A key factor in determining lipid release is the number of ruptured cells located on the six

302   fractured surfaces (faces) of the almond cubes. If $\langle N \rangle$ is the average number of fractured cells

303   in a cube and n_1, n_2, n_3, n_4, n_5, and n_6, represent, respectively, the number of ruptured cells

304   located at each of the 6 faces of the cube, then the following equation can be written:

305 $$\langle N \rangle = n_1 + n_2 + n_3 + n_4 + n_5 + n_6 \tag{7}$$

306   Accordingly, the number of ruptured cells located on each face was determined by dividing

307   the area of a face (p^2) by the area of a circle of diameter d' ($\pi(d'/2)^2$), using eqn (1) to

308   convert profile diameters d' to real diameters d:

309
$$n_1 = n_2 = n_3 = n_4 = n_5 = n_6 = \frac{64p^2}{\pi^3 d^2} \times P \tag{8}$$

310   Therefore when including all six faces:

311
$$\langle N \rangle = \frac{384p^2}{\pi^3 d^2} \times P \tag{9}$$

312   For the STM, the cells at the edges and corners of the faces were unavoidably counted

313   twice and three times, respectively. In the ETM, this anomaly was accounted for by not

314   including the cells that had already been counted on one face on subsequent faces (Fig. 4).

315   Thus, for the number of ruptured cells located on cube faces 1 and 2 (n_1 and n_2, respectively)

316   eqn (8) was used, i.e.

317   Cube faces 1 and 2:

318
$$n_1 = n_2 = \frac{64p^2}{\pi^3 d^2} \times P$$

319   whereas for ruptured cells on cube faces 3 - 6 (n_3 - n_6), it was necessary to use eqn (10) and

320   (11).

321   For cube faces 3 and 4:

322
$$n_3 = n_4 = n_1 - \frac{p}{\frac{\pi}{4}d} \times P \tag{10}$$

323   For cube faces 5 and 6:

324
$$n_5 = n_6 = n_1 - 4P\left[\frac{p}{\frac{\pi}{4}d} - 1\right] \tag{11}$$

325   Thus, for the ETM, eqn (8), (10) and (11) are substituted into eqn (7), to produce the

326   following equation:

327     $$\langle N \rangle = 2\left[\frac{64p^2}{\pi^3 d^2}\right] + 2\left[\frac{64p^2}{\pi^3 d^2} \times P - 2\left(\frac{p}{\frac{\pi}{4}d} \times P\right)\right] + 2\left[\frac{64p^2}{\pi^3 d^2} \times P - 4P\left(\frac{p}{\frac{\pi}{4}d} - 1\right)\right] \quad (12)$$

328   which can be simplified to:

329     $$\langle N \rangle = \frac{384P}{\pi^3}\left(\frac{p}{d}\right)^2 - \frac{48P}{\pi}\left(\frac{p}{d}\right) + 8P \quad (13)$$

330   For both variants of the model, dividing by $\langle N_c \rangle$ then gives the proportion of lipid released

331   from a cube, and the packing density parameter (P) cancels out. Simply multiplying by 100

332   allows all values to be expressed as a percentage. The equations for both variants also

333   included a divisor of 2, because the cutting of the tissue cells creates two faces, so that the

334   lipid released from ruptured cells is shared (50% as a statistical average). Thus, the final

335   equations for the STM and ETM are as follows:

336   <u>STM</u>

337     $$Lipid\ release\ (\%) = \frac{1}{2}\left[\frac{64}{\pi^2}\left(\frac{d}{p}\right)\right] \times 100 \quad (14)$$

338

339   <u>ETM</u>

340     $$Lipid\ release\ (\%) = \frac{1}{2}\left[\frac{64}{\pi^2}\left(\frac{d}{p}\right) - 8\left(\frac{d}{p}\right)^2 + \frac{4}{3}\pi\left(\frac{d}{p}\right)^3\right] \times 100 \quad (15)$$

341   For the STM and ETM variants, it can be seen that lipid bioaccessibility is dependent

342   only on the particle size (p) and real cell diameter (d) of the almond sample. The cell

343   diameter is a constant parameter, since d was determined experimentally; i.e. $d = 36$ μm, after

344   using the Weibel correction in eqn (1). For other plant tissues, d has to be determined

16

345   experimentally using similar methods as employed for almonds. In the final model equations

346   most of the factors considered during initial model construction were not required, and the

347   packing density also became redundant.

3.4. Predictions of bioaccessibility from the theoretical model

349   The lipid release values obtained by STM and the first term of the ETM were identical,

350   (Table 1), because they were the same function of the surface area of the cube; see eqn (14)

351   and (15). Predicted values from both models, expressed as percentage release of the total

352   lipid in the cubes, showed a clear inverse non-linear relationship between the size of cubes

353   and lipid bioaccessibility as the ratio of ruptured to total intact cells increases (Table 1; Fig.

354   5). In Table 1, the lipid release predictions from both models were found to be similar at

355   large cube sizes (> 1 mm), with only slightly higher release values obtained using the STM.

356   Thus, for 2 mm cubes, the proportion of lipid release is predicted to be 5.8 and 5.7%,

357   respectively, from the STM and ETM (Table 1). Values predicted from the two variants of

358   the model diverge more noticeably at cube sizes < 1 mm, with STM values consistently

359   higher than those from the ETM. The higher values obtained from the STM, are not

360   unexpected given that this variant does not include terms that account for shared cells (edge

361   and corner cells) in the theoretical cubes. The unreliability of the STM becomes more serious

362   as the cube sizes decrease to < 500 μm. For example, the lipid release values derived from

363   the STM at cube size 150 μm is ~20% higher than that obtained from the ETM at the same

364   size.

365   The ETM also predicts 100% lipid release for a cube size of ~55 μm (Table 1), which is

366   similar to the dimensions (d) of an individual parenchyma cell (~36 μm). Thus, from eqn (6),

367   the number of cells in a theoretical cube where p = 55 μm, and d = 36 μm, is ~6, which is

368   compatible with 100% lipid release, since all the cells would be theoretically ruptured. On

369   the other hand, the STM predicts, erroneously, 100% release for a theoretical cube size of

370   ~117 μm (Table 1), which is equivalent to a 64-cell cube with ~8 cells potentially still intact.

371   The other important parameter is the average diameter (d) determined for almond

372   parenchyma cells. Its significant effect on lipid release using ETM predictions is clearly seen

373   in Table 2 and plots of cube size (p) versus lipid release at different cell diameters (Fig. 5).

374   Thus at specific cube sizes, the lipid release values predicted from the ETM are higher when

375   larger cell diameters are used, which obviously reflects differences in cell volume. This

376   illustrates the importance of having reliable data on cell size if the model is applied to other

377   plant tissues. The model can also be used to predict the particle size required to produce

378   100% release for a given 'spherical' cell diameter.

379   **3.5. Lipid loss in almond cubes and flour following *in vitro* digestion and comparison of**

380   **lipid digestion values with model predictions of bioaccessibility**

381   To quantify the extent of lipid digestion in the laboratory, 2 mm almond cubes and almond

382   flour, which exhibit low and high lipid bioaccessibility, respectively, were digested under

383   simulated gastric and duodenal conditions for 3h.[21] The size of the cubes post-digestion

384   appeared to remain more or less the same, indicating that there had been negligible

385   disintegration or swelling of the cube samples during digestion. The total loss of lipid by

386   hydrolysis post-digestion as a percentage of the original lipid content in the cubes and flour,

387   was found to be 9.9 ± 0.71% and 39.3 ± 0.18% (mean ± SD, n = 4), respectively. As

388   discussed above, the proportion of lipid released from the ruptured cells of the cut surface of

389   the 2 mm almond cubes, as predicted from the ETM, was 5.7% (Table 1). Lipid release

390   predicted from the model for almond flour was 42%, which is based on a pooled mean

391   particle size of 225 μm (see methods section 2.2). For mean particle sizes obtained from the

392   suppliers (200 µm) and determined in the laboratory (250 µm), the predicted bioaccessibility

393   values were 46 and 39 %, respectively.

4. Discussion

395   Previous studies of almonds and other plant tissues have highlighted the importance of the

396   structural integrity and behaviour of cell walls in regulating the release and digestion of lipid

397   and other macronutrients.[20,21,23] Thus in almond tissue, lipid that is encapsulated by intact

398   cell walls is much less available for digestion than lipid released from ruptured cells and

399   exposed to digestive fluids in the gut lumen. Also, the relationship between almond structure

400   and lipid bioaccessibility has also received serious attention with respect to its impact on gut

401   hormone secretion, energy metabolism, appetite/satiety and masticatory performance.[36,44,45]

402   Moreover, the importance of the cell wall barrier mechanism in restricting the digestion of

403   lipid and other macronutrients[20-21] provides a plausible explanation, *inter alia*, of why the

404   Atwater system is unreliable for predicting the metabolisable energy (ME) of many plant

405   foods. Recent data shows that Atwater factors overestimate the ME of almonds by as much

406   as 32%.[32]

407   In previous studies we have shown that trituration of almonds by mechanical processing

408   or mastication increases the release of lipid from almond cells as a result of cell wall

409   rupture.[20,21,36] The current study was designed to quantify the effects of cell wall rupture on

410   lipid bioaccessibility in almond tissue. Our results show that the amount of lipid release is

411   mainly a function of the number of ruptured cells on the fractured surface of almond tissue

412   and that this physical release of 'free' lipid increases its susceptibility to lipolysis in the early

413   stages of digestion. Not surprisingly, the ratio of ruptured cells to intact cells is inversely

414   related to particle (cube) size, as predicted by the theoretical model. It is worth noting that

415   the almond cell walls contain predominantly pectic material (>60%), with seemingly smaller

416 amounts of xyloglucan, xylan and cellulose.[11,20,42] This suggests that the almond cells have

417 the potential capacity to separate during cooking, producing separated cells with encapsulated

418 lipid. Cell separation is caused mainly by the depolymerisation and solubilisation of pectin in

419 the middle lamella.[3] However, in none of the studies we have performed so far, [20,21,36]

420 including the current one, has there been any evidence of cell separation occurring in raw or

421 heat processed almonds that have been cut, pulverised or masticated, except in ingested

422 almonds after microbial fermentation *in vivo*.[20]

423 In this paper, two variants of a theoretical model were constructed for predicting lipid

424 release from ruptured cells of almond cotyledon; one model is based on predictions of cell

425 rupture on the six surfaces of the cube (STM), and the other model includes additional terms

426 that take into account cell sharing at edges and corners (ETM). The ETM shows considerable

427 promise for predicting the release of lipid and other nutrients, especially since it allows

428 reliable predictions of bioaccessibility to be made over a broad range of particle and cell

429 sizes, which is not the case for the STM. Lipid bioaccessibility of the almond samples was

430 not determined experimentally in the current study. However, in a recent study, we used a

431 solvent extraction method to estimate lipid release in raw almonds masticated by healthy

432 human volunteers.[36] The empirical results were then compared with predictions of

433 bioaccessibility by applying particle size data of masticated almonds to the ETM. The mean

434 value for lipid release was found to be $7.9 \pm 0.7\%$ ($\pm$SEM), which compared favourably with

435 a mean value of $8.5 \pm 0.7\%$ predicted from the model.

436 The lipid loss values produced from *in vitro* digestion of the almond cubes and finely

437 ground flour were consistent with predictions of lipid bioaccessibility, with the flour showing

438 a 4-fold increase in lipid loss relative to the 2 mm cubes. The much higher lipid loss

439 observed for flour can be explained by the substantially lower particle size of the flour and

440 therefore larger number of ruptured cells with exposed '*free*' lipid on the fractured surfaces of

441   almond particles, as previously observed.[20,21] The *in vitro* digestion value obtained for

442   almond cubes was ~4% higher than the model prediction for lipid bioaccessibility and a

443   number of factors may explain this difference.

444   One possible factor is that the cutting method used for preparing large numbers of almond

445   cubes for the digestion assay, albeit carefully performed, may have produced cubes with

446   dimensions slightly < 2 mm. Predicted bioaccessibility values based on 1.5 and 1 mm cubes

447   are 7.6 and 11.2%, respectively. A second factor is that it is possible that the cubes were

448   physically disrupted during *in vitro* digestion, thereby reducing their particle size. There was

449   no evidence to indicate however that the almond cubes disintegrated during *in vitr*o digestion.

450   Also, evidence of disruption post-digestion was not observed *in vivo*,[21] although microbial

451   erosion of almonds in the large intestine is highly likely.[20,46] An additional factor may be the

452   introduction of small cracks/fissures into the cell walls during cutting, which propagate from

453   cells on the cube surface into cells underlying the fractured surface. These cracks could

454   allow lipid to leach out of damaged cells into the aqueous phase of digesta and/or to be

455   digested by lipase *in situ* followed by leakage of the hydrolysed products. If an entire

456   secondary cell layer was ruptured, lipid release would be almost doubled. Nevertheless,

457   examination of fractured surfaces of almonds, including those of cut cubes, before and after

458   digestion (*in vitro* and *in vivo*) has not provided any evidence of significant levels of

459   fissuring,[21] though further work on this aspect is certainly warranted. Micrographs of the cut

460   surface of an almond cube clearly show the cell rupture of surface cells with little damage to

461   the underlying cells (see Electronic Supplementary Information). One final factor may be the

462   possible increase in the porosity of the cell wall matrix during digestion and, therefore,

463   perhaps influx of lipase and subsequent leakage of hydrolysed products of lipid.[21]

464   Some evidence for lipid loss from intact cells in almond cubes was reported in a pilot *in*

465   *vivo* study, in which ileostomy volunteers swallowed cubes without chewing and then

466   effluent was collected postprandially at the end of the small intestine.[21] However, the loss of

467   encapsulated lipid appeared to occur more slowly and at much longer digestion times (i.e. 3-

468   12h) in the upper gut than the incubation times used for *in vitro* digestion. Furthermore,

469   analysis of the ileostomy effluent suggested that intra-cellular lipid was lost from seemingly

470   intact parenchyma cells underlying the fractured cell layers. This process would involve

471   inward diffusion of digestive fluids containing lipase, colipase and bile salts through the cell

472   wall barrier and subsequent outward movement of products of lipolysis into the digestive

473   milieu. The apparent increase in porosity may occur as a result of swelling of the cell wall

474   matrix during digestion, which was also observed in the ileostomy study.[21]

475   Only lipid released from broken cells at the cut surface of almond cubes, as predicted by

476   the ETM, seems to be susceptible to hydrolysis during the early digestion phase and is

477   therefore available for absorption, contributing to the postprandial rise in plasma

478   triacylglycerol (TAG) concentrations. Moreover, the time course of early digestion of

479   bioaccessible lipid matches fairly closely the peak rise in TAG (3-4 h), and is therefore of

480   physiological importance.[16] Evidence continues to emerge also about the importance of

481   postprandial TAG concentrations as a significant diet-related risk factor for CHD.[28] The

482   ETM has potential use for not only predicting lipid release post-mastication, but also for

483   predicting subsequent effects on post-absorptive metabolism.[20,44] Some evidence for this

484   arises from our recent study to predict, from particle size data of ingested almonds, the effects

485   of lipid release on postprandial lipaemia in healthy humans.[16] The main finding from this

486   study was that the amount of lipid released from ruptured almond cells plays a key role in

487   influencing postprandial lipaemia.

488   The mastication process has a major impact on early lipid release from fractured cell

489   layers of almonds, since the extent of oral processing determines the number of ruptured cells

490   on the particle surface.[20,44] Predictive modelling could be used therefore to estimate lipid

22

491 bioaccessibility of masticated almonds and similar foods, even though masticated food

492 particles are usually heterogeneous in shape and size.[20,44,47-49] In the case of masticated

493 almonds, the very broad size distributions, mostly range from 5 μm to 4 mm.[36,44,49] We

494 recently demonstrated the efficacy of the ETM for predicting lipid release using data from

495 particle size analysis of masticated almonds.[36] This involved combining laser diffraction and

496 mechanical sieving methods to cover the wide range of particle sizes found in almond

497 boluses.

498 In future studies, an important test of the theoretical model will be whether it can be

499 applied more universally for predicting the bioaccessibility of nutrients other than lipid, not

500 just in almonds but also in other plant foods. Recent work suggests that the application of the

501 model to other nutrients, e.g. proteins and vitamin E, is likely to be worthwhile.[20,21] Although

502 the ETM has yet to be evaluated in other plant foods, materials with similar histology, texture

503 and fracture properties during mastication and processing, such as other oil-bearing edible

504 seeds, are worthy of study. The model could also be applied to other types of plant

505 seeds/grains, but differences in shape, dimensions and properties of the cells and cell walls

506 would have to be accounted for. This would be particularly relevant to plant structures where

507 there is evidence of cell wall rupture during mastication and mechanical processing (e.g.

508 milling).

509 5. Conclusions

510 We have constructed two variants of a mathematical model for predicting lipid

511 bioaccessibility from the ruptured cells of almond cotyledonary tissue, based on estimating

512 the number of ruptured cells in a theoretical almond cube. Both variants shared key

513 parameters, namely the cell diameter and the particle (cube) size. However, only the ETM

514 was acceptable for predicting lipid bioaccessibility in almond particles with a broad range of

515   particle sizes. For this reason, the ETM has the potential to be applied to heterogeneous

516   almond particles produced by mechanical processing (e.g. milling) or mastication *in vivo*.

517   Recent evidence for the validity of this predictive model has come from the results of a

518   mastication study in human subjects in which lipid release was estimated from the ETM

519   using size distribution data of chewed particles.[36]

520   Furthermore, *in vitro* digestion of almond cubes and flour, which exhibit low and high

521   lipid bioaccessibility, respectively, showed that the lipid released from ruptured almond cells

522   was available for hydrolysis. It seems reasonable to conclude therefore that the ETM has

523   potential use for predicting lipid release in almonds during the early phase of digestion in the

524   upper GI tract and, as previously reported, for the prediction of postprandial lipaemia.[16] The

525   application of this model to studies of cell wall rupture in other edible plant materials will

526   provide further insight of the mechanisms by which dietary fibre regulates nutrient release

527   and gut function.

528   ## Acknowledgements

24

References

1. I. A. Brownlee, *Food Hydrocolloid.*, 2011, **25**, 238-250.

2. P. A. Judd and P. R. Ellis, in *Traditional Medicines for Modern Times*, ed. A. Soumyanath, CRC Press, Boca Raton, 2005. pp. 257-272.

3. K. W. Waldron, M. L. Parker and A. C. Smith, *Compr. Rev. Food Sci. Food Saf.*, 2003, **2**, 128-146.

4. J. M. Pinos-Rodríguez, S. S. González, G. D. Mendoza, R. Bárcena, M. A. Cobos, A. Hernández and M. E. Ortega, *J. Anim. Sci.*, 2002, **80**, 3016-3020.

5. R. N. Carmody, G. S. Weintraub and R. W. Wrangham, *P. Natl. Acad. Sci. USA*, 2011, **108**, 19199–19203.

6. M. M. Wollstonecroft, P. R. Ellis, G. C. Hillman and D. Q. Fuller, *Veg. Hist. Archaeobot.*, 2008, **17**, S19-S27.

7. M. M. Wollstonecroft, P. R. Ellis, G. C. Hillman, D. Q. Fuller and P. J. Butterworth, *P. Natl. Acad. Sci. USA*, 2012, **109**, E991.

8. D. B. Jordan, M. J. Bowman, J. D. Braker, B. S. Dien, R. E. Hector, C. C. Lee, J. A. Mertens and K. Wagschal, *Biochem. J.*, 2012, **442**, 241-252.

9. M. Pauly and K. Keegstra, *The Plant Journal*, 2008, **54**, 559-568.

10. I. Burgert, *Am. J. Bot.*, 2006, **93**, 1391-1401.

11. T. Grassby, C. H. Edwards, M. Grundy and P. R. Ellis, in *Stability of complex Carbohydrate Structures:Biofuels, Foods, Vaccines and Shipwrecks*, ed. S. E. Harding, Royal Society of Chemistry, 2013, ch. 4, pp. 36-55.

12. S. Posé, A. R. Kirby, J. A. Mercado, V. J. Morris and M. A. Quesada, *Carbohyd. Polym.* 2012, **88**, 882-890.

13. Q. Wang, P. R. Ellis and S. B. Ross-Murphy, *Carbohyd. Polym.*, 2006, **64**, 239-246.

14. Q. Wang, P. R. Ellis and S. B. Ross-Murphy, *Carbohyd. Polym.*, 2008, **74**, 519-526.

15. M. C. Jarvis, *Food Hydrocolloid.*, 2011, **25**, 257-262.

16. S. E. E. Berry, E. A. Tydeman, H. B. Lewis, R. Phalora, J. Rosborough, D. R. Picout and P. R. Ellis. *Am. J. Clin. Nutr.*, 2008, **88**, 922-929.

17. A. P. Gunning, R. J. M. Bongaerts and V. J. Morris, *FASEB Journal,* 2009, **23**, 415–424.

18. W. Stahl, H. van den Berg, J. Arthur, A. Bast, J. Dainty, R. M. Faulks, C. Gärtner, G. Haenen, P. Hollman, B. Holst, F. J. Kelly, M. C. Polidori, C. Rice-Evans, S. Southon, T. van Vliet, J. Viña-Ribes, G. Williamson and S. B. Astley, *Mol. Aspects Med.*, 2002, **23**, 39-100.

19. E. A. Tydeman, M. L. Parker, R. M. Faulks, K. L. Cross, A. Fillery-Travis, M. J. Gidley, G. T. Rich and K. W. Waldron, *J. Agric. Food Chem.*, 2010, **58**, 9855-9860.

20. P. R. Ellis, C. W. C. Kendall, Y. L. Ren, C. Parker, J. F. Pacy, K. W. Waldron and D. J. A. Jenkins, *Am. J. Clin. Nutr.*, 2004, **80**, 604-613.

21. G. Mandalari, R. Faulks, G. T. Rich, V. Lo Turco, D. Picout, R. B. Lo Curto, C. Bisignano, G. Dugo, K. W. Waldron, P. Ellis and M. S. Wickham, *J. Agric. Food Chem.*, 2008, **56**, 3409-3416.

22. G. Livesey, J. A. Wilkinson, M. Roe, R. Faulks, S. Clark, J. C. Brown and H. Kennedy, M. Elia, *Am. J. Clin. Nutr.*, 1995, **61**, 75-81.

23. L. Noah, F. Guillon, B. Bouchet, A. Buléon, C. Molis, M. Gratas and M. Champ, *J. Nutr.*, 1998, **128**, 977-985.

26

24. J. Parada, J. M. Aguilera, *J. Food Sci.*, 2007, **72**, R21-R32.

25. D. J. A. Jenkins, C. W. C. Kendall, A. Marchie, T. L. Parker, P. W. Connelly, W. Qian, J.
    S. Haight, D. Faulkner, E. Vidgen, K. G. Lapsley and G. A. Spiller, *Circulation*, 2002,
    106, 1327-1332.

26. D. J. A. Jenkins, C. W. C. Kendall, A. R. Josse, S. Salvatore, F. Brighenti, L. S. A.
    Augustin, P.R. Ellis, E. Vidgen and V. Rao, *J. Nutr.*, 2006, **136**, 1-6.

27. A. R. Josse, C. W. C. Kendall, L. S. Augustin, P. R. Ellis and D. J. A. Jenkins,
    Metabolism, 2007, **56**, 400-404.

28. K. G. Jackson, S. D. Poppitt and A. M. Minihane, *Atherosclerosis*, 2012, **220**, 22-33.

29. J. Hollis and R. Mattes, *Brit. J. Nutr.*, 2007, **98**, 651-656.

30. S. Rajaram and J. Sabaté, *Brit. J. Nutr.*, 2006, **96**, S79-S86.

31. M. A. Wien, J. M. Sabaté, D. N. Iklé, S.E. Cole and F. R. Kandeel, *Int. J. Obesity*, 2003,
    27, 1365-1372.

32. J. A. Novotny, S. K. Gebauer and D. J. Baer, *Am. J. Clin. Nutr.*, 2012, **96**, 296-301.

33. P. W. J. Maljaars, H. P. F. Peters, D. J. Mela and A. M. M. Masclee, *Physiol. Behav.*
    2008, **95**, 271-281.

34. O. Döker, U. Salgin, N. Yildiz, M. Aydoğmuş and A. Çalimli, *J. Food Eng.*, 2010, **97**,
    360–366.

35. L. Fiori, *J. Supercrit. Fluid.*, 2009, **50**, 218–224.

36. M. M. L. Grundy, T. Grassby, G. Mandalari, K. W. Waldron, P. J. Butterworth, S. E. E.
    Berry, P. R. Ellis, *Am. J. Clin. Nutr.*, (in press)

37. E. R. Weibel, in *Practical Methods for Biological Morphometry*, Academic Press, London, 1979, vol. 1, ch. 2.

38. H. S. M. Coxeter, *Introduction to Geometry*, New York: Wiley, 1961.

39. M. Goldberg, *Math. Mag.*, 1971, **44**, 199-208.

40. C. Siefe, *Science*, 2000, **287**, 1910-1912.

41. Anon, *The Merck Index*, ed. M. Windholz, S. Budavari, 9th edn., Merck Co Inc; 1976.

42. F. Dourado, A. Barros, M. Mota, M. A. Coimbra and F. M. Gama, *J. Agric. Food Chem.*, 2004, **52**, 1364-1370.

43. C. T. Young, W. E. Schadel, H. E. Pattee and T. H. Sanders, *LWT - Food Sci. Technol.*, 2004, **37**, 317-322.

44. B. A. Cassady, J. H. Hollis, A. D. Fulford, R. V. Considine and R. D. Mattes, *Am. J. Clin. Nutr.*, 2009, **89**, 794-800.

45. J. M. Frecka, J. H. Hollis and R. D. Mattes, *Eur. J. Clin. Nutr.*, 2008, **62**, 1231-1238.

46. G. Mandalari, C. Nueno-Palop, G. Bisignano, M. S. J. Wickham and A. Narbad, *Appl. Environ. Microbiol.*, 2008, **74**, 4264-4270.

47. M. L. Jalabert-Malbos, A. Mishellany-Dutour, A. Woda and M.-A. Peyron, *Food Qual. Prefer.*, 2007, **18**, 803-812.

48. A. Mishellany, A. Woda, R. Labas and M. A. Peyron, *Dysphagia*, 2006, **21**, 87-94.

49. M.-A. Peyron, A. Mishellany and A. Woda, *J. Dent. Res.*, 2004, **83**, 578-582.

Table 1   Comparison of the percentage lipid release predicted by the Simple Theoretical Model (STM) and the Extended Theoretical Model (ETM) for a wide range of almond cube sizes. Measured mean cell profile diameter, $d' = 28.3\mu m$ was used to calculate the cell diameter, $d = 36$ μm.

Particle edge length		Simple Theoretical Model (STM)				Extended Theoretical Model (ETM)				
		Total no. of cells	Total ruptured cells	Lipid fraction	Lipid %	1st term	2nd term	3rd term	Lipid fraction	Lipid %
p (μm)	d/p	$\langle N_c \rangle$	$\langle N \rangle$	$\langle N \rangle / \langle N_c \rangle$		F	E	V	$F-E+V$	
5000	0.007	5102955	119234	0.02	2.3	0.02	0.00	0.00	0.02	2.3
4000	0.009	2612713	76309	0.03	2.9	0.03	0.00	0.00	0.03	2.9
3350	0.011	1534780	53524	0.03	3.5	0.03	0.00	0.00	0.03	3.4
3000	0.012	1102238	42924	0.04	3.9	0.04	0.00	0.00	0.04	3.8
2000	0.018	326589	19077	0.06	5.8	0.06	0.00	0.00	0.06	5.7
1700	0.021	200567	13783	0.07	6.9	0.07	0.00	0.00	0.07	6.7
1400	0.026	112020	9348	0.08	8.3	0.08	0.00	0.00	0.08	8.1
1000	0.036	40824	4769	0.12	11.7	0.12	0.01	0.00	0.11	11.2
850	0.042	25071	3446	0.14	13.7	0.14	0.01	0.00	0.13	13.0
700	0.051	14003	2337	0.17	16.7	0.17	0.01	0.00	0.16	15.7
500	0.072	5103	1192	0.23	23.4	0.23	0.02	0.00	0.21	21.4
250	0.144	638	298	0.47	46.7	0.47	0.08	0.01	0.39	39.1
200	0.180	327	191	0.58	58.4	0.58	0.13	0.01	0.47	46.7
150	0.240	138	107	0.78	77.9	0.78	0.23	0.03	0.58	57.7
125	0.288	80	75	0.93	93.5	0.93	0.33	0.05	0.65	65.2
100	0.360	41	48	1.17	>100	1.17	0.52	0.10	0.75	74.7
70	0.515	14	23	1.67	>100	1.67	1.06	0.29	0.89	89.5
60	0.601	9	17	1.95	>100	1.95	1.44	0.45	0.96	95.8
55	0.655	7	14	2.12	>100	2.12	1.72	0.59	1.00	99.6
50	0.721	5	12	2.34	>100	2.34	2.08	0.78	1.04	>100
40	0.901	3	8	2.92	>100	2.92	3.25	1.53	1.21	>100
30	1.201	1	4	3.89	>100	3.89	5.77	3.63	1.75	>100

Table 2　Effect of changing cell diameter (d) on predicted lipid release (%) for five different almond cube sizes p =100 µm, p = 250 µm, p = 500 µm, p = 1000 µm, and p = 2000 µm.

538

d (µm)	Lipid release (%)				
	p =100 µm	p = 250 µm	p = 500 µm	p = 1000 µm	p = 2000 µm
15	40.3	18.1	9.4	4.8	2.4
20	50.5	23.5	12.3	6.3	3.2
25	59.3	28.6	15.2	7.9	4.0
30	66.9	33.5	18.1	9.4	4.8
35	73.5	38.1	20.8	10.9	5.6
40	79.1	42.5	23.5	12.3	6.3
50	88.3	50.5	28.6	15.2	7.9
55	92.2	54.2	31.1	16.7	8.6
60	95.8	57.7	33.5	18.1	9.4
70	>100	64.0	38.1	20.8	10.9
80	>100	69.7	42.5	23.5	12.3
90	>100	74.7	46.6	26.1	13.8
100	>100	79.1	50.5	28.6	15.2
110	>100	83.1	54.2	31.1	16.7
120	>100	86.6	57.7	33.5	18.1
130	>100	89.9	60.9	35.9	19.4
140	>100	92.9	64.0	38.1	20.8
150	>100	95.8	66.9	40.3	22.2
170	>100	>100	72.2	44.6	24.8
200	>100	>100	79.1	50.5	28.6

Figures

Fig. 1 A schematic illustration of an almond seed and a cubic sample of the almond tissue (cotyledon) showing the fractured cell surfaces of the cut tissue. The surfaces of the cube show a superimposed micrograph (created approximately to scale) produced by scanning electron microscopy, previously prepared from a section of almond cotyledon. The large round structures are lipid droplets produced from coalesced lipid bodies, originating from the ruptured parenchyma cells. A full description of these micrographs is given by Ellis et al.[20]

~ 0.25 mm
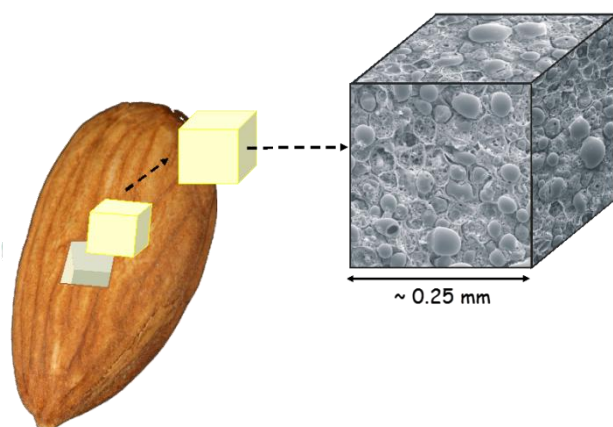
Fig. 2   Schematic illustration of a cut section of a 'spherical' cell, representing the pseudo-spherical geometry of a parenchyma cell of almond cotyledon, cut at different locations of the sphere. The profile diameter ($d' = 2 \times r'$), which is less than or equal to the real diameter, varies depending on the location of the cut surface (i.e. equator or displaced towards the poles). This can be accounted for using stereological principles; see eqn (1).[36]
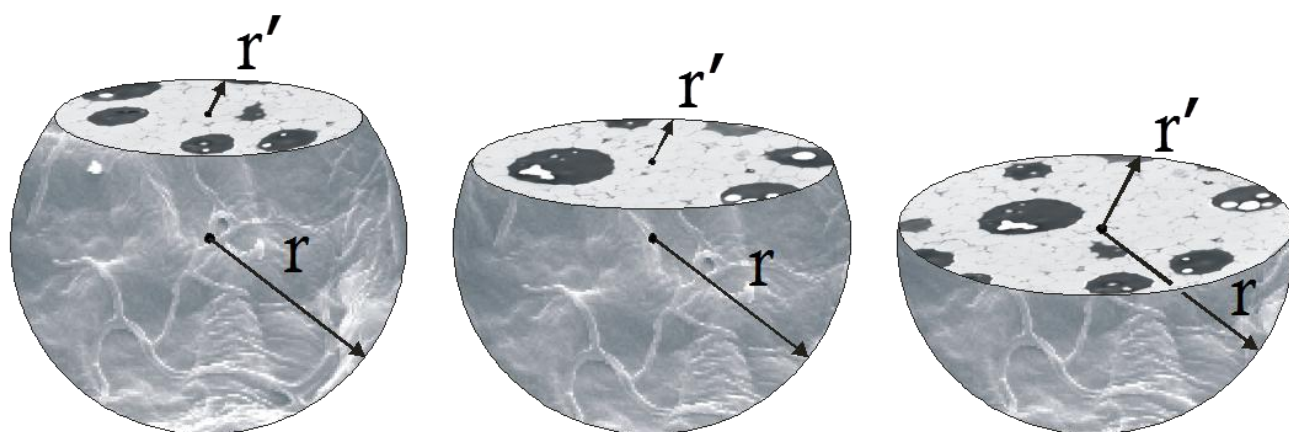
Fig. 3　　(a) Light microscopy section of parenchyma cells of almond cotyledon tissue stained with toluidine blue to locate cell walls and intra-cellular components. The micrograph provided information about the size and shape of the parenchyma cells. Scale bar for the micrograph = 20 μm. (b) Image analysis of a micrograph of a single parenchyma cell, produced by transmission electron microscopy of almond cotyledon tissue, and used for estimating the lipid content of individual cells. The lipid area, seen as lipid bodies of ~1-3 μm, was calculated as the difference between the total surface area of the cell and the surface area of non-lipid components (e.g. protein inclusions seen as darker regions), and expressed as a percentage of the total cell surface area. Scale bar = 5 μm.
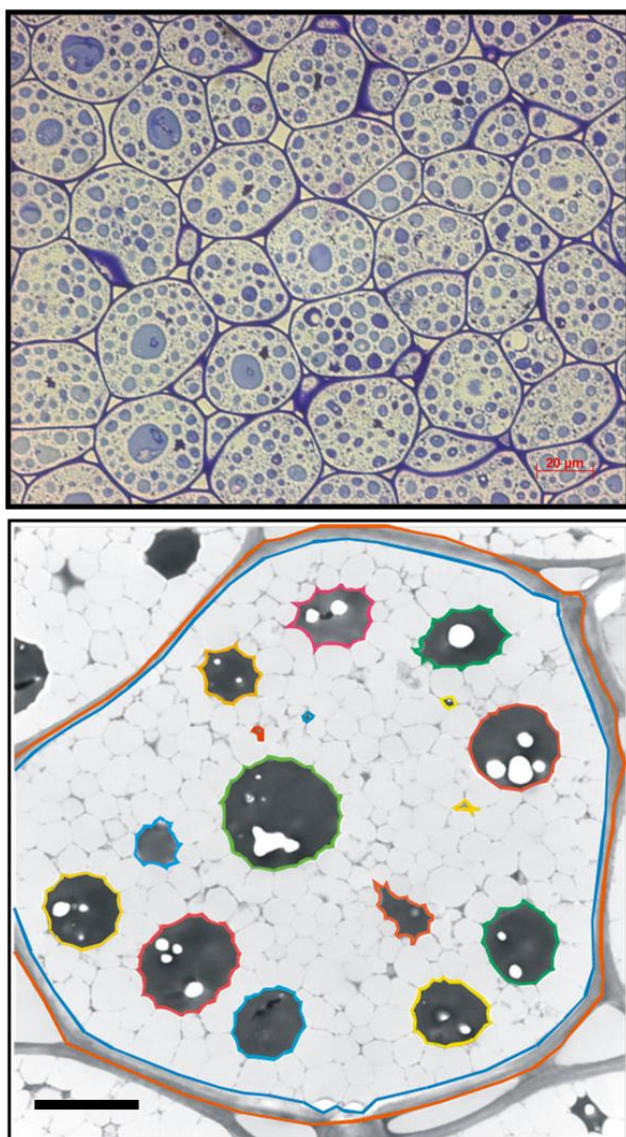
Fig. 4   Schematic illustration of the packing arrangement of cells at the surface of a cube;

the cells represent the pseudo-spherical parenchyma cells in a cut cube of almond cotyledon.

The cells at the surface of a cut cube of almond tissue are fractured. Cells at the edges and

corners of the cube share 2 and 3 surface faces, respectively.
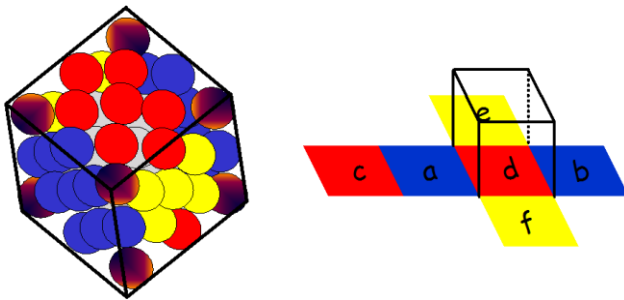
Fig. 5 A double logarithmic plot, derived from eqn (15), of particle size versus percentage lipid release. The blue line can be used for predicting lipid release from parenchyma cells of almond cotyledon with real average cell diameters of 36 µm. The purple, brown and green lines represent particle size-lipid release plots of cell diameters 20, 50 and 100 µm and show the significant changes in lipid release.